TECHNICAL RESEARCH REPORT

Representation of Spectral Profiles in the Auditory System
II: Detection of Spectral Peak Shape Changes

by S. Vranic - Sowers and S.A. Shamma

T.R. 94-15

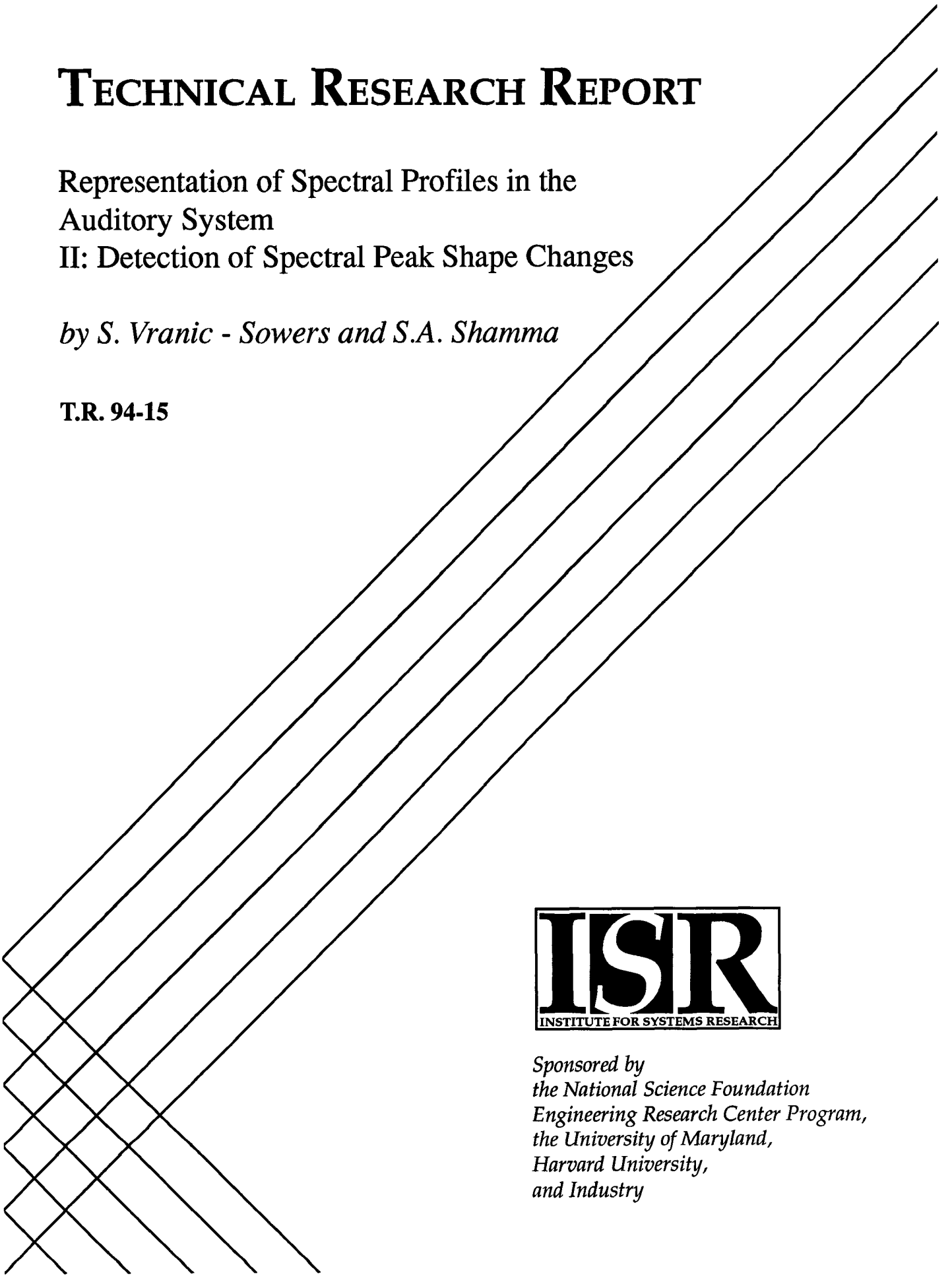

Sponsored by
the National Science Foundation
Engineering Research Center Program,
the University of Maryland,
Harvard University,
and Industry

Representation of spectral profiles in the auditory system. II: Detection of spectral peak shape changes.

Svetlana Vranić - Sowers
Department of Electrical Engineering and Institute for Systems Research,
University of Maryland, College Park, MD 20742, U.S.A.

Shihab A. Shamma
Department of Electrical Engineering, Institute for Systems Research,
and University of Maryland Institute for Advanced Computer Studies,
University of Maryland, College Park, MD 20742, U.S.A.

Received:

Short title: **Detection of spectral peak shape changes.**

Abstract

Based on the ripple analysis model outlined in Part I of this paper, predictions are made for the detection of shape changes in spectral peak profiles. Peak shape is uniquely described in terms of two parameters: bandwidth factor (BWF) which reflects the tuning or sharpness of a peak, and a symmetry factor (SF) which roughly measures the local evenness or oddness of a peak. Using profile analysis methods, thresholds to changes in these parameters (defined as δBWF/BWF and δSF) are measured together with the effects of several manipulations such as using different peak levels, varying spectral component densities, and randomizing the frequencies of the peaks. The new ripple analysis model accounts well for the measured thresholds. Predictions of the three previously published models for the same profiles are also evaluated and discussed.

INTRODUCTION

The shape of the acoustic spectrum is a fundamental cue in the perception and recognition of complex sounds. It is, however, uncertain how this spectrum is represented in the auditory system and what specific features are extracted and emphasized by such a representation. In Part I of this paper [*Vranić-Sowers and Shamma*, 19xx], it is proposed that the auditory system transforms the spectral profile into a weighted sum of sinusoidal spectra – called ripples. This ripple analysis is carried out by a bank of filters tuned to ripples of different frequencies and phases. Perception of the profile is then based on the ripple transform of the profile and not on the profile itself. This hypothesis is partly supported by physiological data demonstrating that the primary auditory cortex (AI) is indeed capable of carrying out the ripple analysis implied by the model [*Calhoun and Schreiner*, 1993; *Shamma, Versnel and Kowalski*, 1993].

To test this hypothesis, a computational model was developed and applied successfully to the prediction of perceptual thresholds of several well known profile analysis experiments [*Vranić-Sowers and Shamma*, 19xx]. However, to distinguish this model from other profile analysis models (e.g., the maximum difference [*Bernstein and Green*, 1987] and the independent channels models [*Durlach, Braida and Ito*, 1986]), several predictions were made regarding the detection of complex changes in arbitrary profiles [*Vranić-Sowers and Shamma*, 19xx]. The most important is that sensitivity to shifts in the "magnitude" and "phase" of the ripple transform of an arbitrary profile should be comparable, respectively, to the frequency-difference-limen (**fdl**) and phase-difference-limen (**pdl**) thresholds measured with single ripple profiles [*Green*, 1986; *Hillier*, 1991; *Vranić-Sowers and Shamma*, 19xx].

These predictions are tested here using a spectral peak profile similar to a vowel formant. Subjects' sensitivities to ripple transform shifts are estimated from their perceptual thresholds to changes in several peak shape parameters. Results are then

compared to predictions from the ripple analysis model and also from the independent channels model [*Durlach, Braida and Ito*, 1986], the maximum difference model [*Bernstein and Green*, 1987], and the Ewaif model [*Stover and Feth*, 1983].

In the following section (Sec. I), the acoustic stimuli are described in detail and their ripple transforms are computed. In Sec. II, changes in peak's bandwidth, symmetry, and amplitude are interpreted in the ripple transform domain, respectively, as **fdl-**, **pdl-**, and pedestal-type experiments, in the sense defined in Part I of this paper [*Vranić-Sowers and Shamma*, 19xx], and detection thresholds for these three types of experiments are predicted for spectral peak profiles. In Sec. III, experimental results are reported and compared to predictions of the ripple analysis model. Predictions of the three alternative models for the same experiments and further general discussion of the results are presented in Secs. IV and V, respectively.

I. DESCRIPTION OF THE PEAK PROFILES

A. Spectral peak stimulus parameters

The peak profile was defined as the envelope of a broadband stimulus consisting of N components equally spaced on a logarithmic frequency axis (ω), where $\omega = \log_2(f/f_o)$ octaves, f is the frequency (in kHz), and f_o is the frequency of the largest peak component (Fig. 1(a)). The stimulus spectrum consisted of two portions, the base and the peak. The base components were all equal in amplitude and they were added in phase to peak components of different symmetries and bandwidths to form the peak profiles. The peak profile is defined in terms of the following parameters (Fig. 1(a)):

- ω_o is the location of the peak's maximum.
- S is the slope of the profile near the peak's maximum (in dB/octave). For $\omega \leq \omega_o$, $S = L$ (the left slope), and for $\omega > \omega_o$, $S = R$ (the right slope).
- $b(\omega) = b$ is the flat base of the peak profile.
- $a(\omega) = a_{max} \cdot 10^{\frac{S}{20}(\omega-\omega_o)}$, is the amplitude of the peak portion of the profile. a_{max} is the maximum amplitude of the peak profile (at $\omega = \omega_o$). It is also defined in dB as $A_{max} = 20\ \log_{10}(\frac{a_{max}}{b})$.

Therefore, the overall peak profile (on a linear scale) is given by:

$$p(\omega) = b(\omega) + a(\omega) = b + a_{max}10^{\frac{S}{20}(\omega-\omega_o)},$$

and on a dB scale:

$$p_{dB}(\omega) = 20\ \log_{10}(b + a_{max}10^{\frac{S}{20}(\omega-\omega_o)}) = 20\ \log_{10}(b\ (1 + 10^{\frac{A_{max}}{20}+\frac{S}{20}(\omega-\omega_o)})).$$

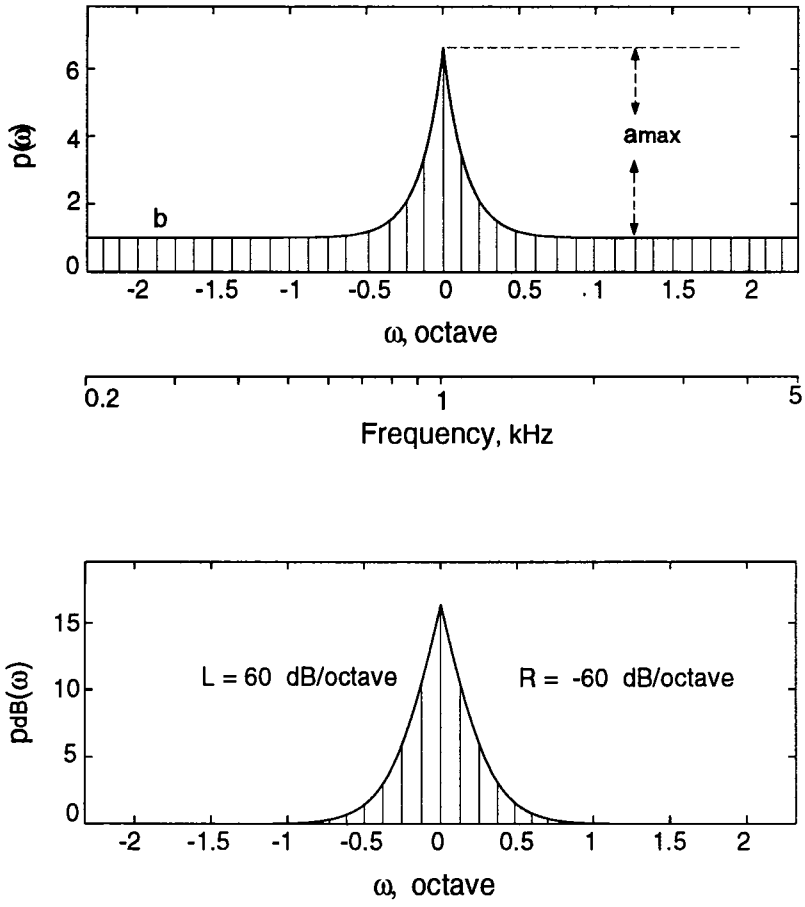

Figure 1: (a) Peak profile plotted on a linear (top) and logarithmic (bottom) amplitude scale. Peak level (A_{max}) is 15 dB, and BWF = 0.1 octave and SF = 0.

For example, the peak in Fig. 1(a) is 15 dB in level (A_{max}) with slopes $L = 60$ dB/octave and $R = -60$ dB/octave around the peak. Note that around ω_o the peak profile can be approximated by:

$$p_{dB}(\omega) \approx 20\ \log_{10}(b \cdot 10^{\frac{A_{max}}{20} + \frac{S}{20}(\omega - \omega_o)}) = 20\ \log_{10} b\ +\ A_{max}\ +\ S(\omega - \omega_o),$$

i.e., the peak has approximately a triangular profile as shown in Fig. 1(a) (lower panel).

In all experimental conditions, standard and signal consisted of $N = 11$, 21, or 41 zero phase components equally spaced on a logarithmic scale between 0.2–5 kHz (ω in the range ± 2.32 octave), with the peak always centered at 1 kHz ($\omega_o = 0$ octave). The amplitude of each component p_i in the stimulus can be computed from:

$$p_i = b + a_{max} 10^{l(i - i_o)},\ \text{for } i \leq i_o,$$

and

$$p_i = b + a_{max} 10^{r(i - i_o)},\ \text{for } i > i_o,$$

where i is the component index, i_o is the index of the largest peak component, $l = (L/20) \cdot (M/N)$, $r = (R/20) \cdot (M/N)$, and M is the frequency range of the spectrum in octaves ($M = 4.64$ octave). For our centered peaks, $i_o = (N + 1)/2$.

No other (than zero) phase conditions were tested since numerous previous experiments have shown that phase effects on signal detection are minimal ([*Bernstein, Richards and Green*, 1987; *Green and Mason*, 1985]).

B. Peak shape parameters

In order to describe its shape efficiently, a peak profile was parametrized uniquely in terms of a bandwidth factor (BWF) and a symmetry factor (SF). BWF is the bandwidth of the peak (measured at 3 dB's below the peak) and is defined as: BWF = 3 (1/L - 1/R) octave. The SF represents the percentage difference of the slopes around the peak and is defined as: SF = (L + R) / (L - R). For instance, the peak in Fig. 1(a) has BWF = 0.1 octave and SF = 0. Peaks with various other BWF's and SF's are shown in Fig. 1(b) covering the full range of profiles used in our experiments. Conversely, given any BWF and SF, the slopes around the peak can be computed as: R = -6/(BWF (1 + SF)) dB/octave, and L = 6/(BWF (1 - SF)) dB/octave. A third parameter – the peak level (A_{max}) is also required to define the peak completely with respect to the baseline.

To make the spectral peaks asymmetric, they were always tilted towards higher frequencies (or to the right). This, together with choosing the peak frequency at 1 kHz and limiting the range of BWF values under 0.4 octave, ensured that the spectral peaks were located above 500 Hz where the cochlear frequency axis is assumed largely logarithmic. This is an important consideration since the peak shapes used were explicitly defined in terms of spectral slopes along such an axis. The largest

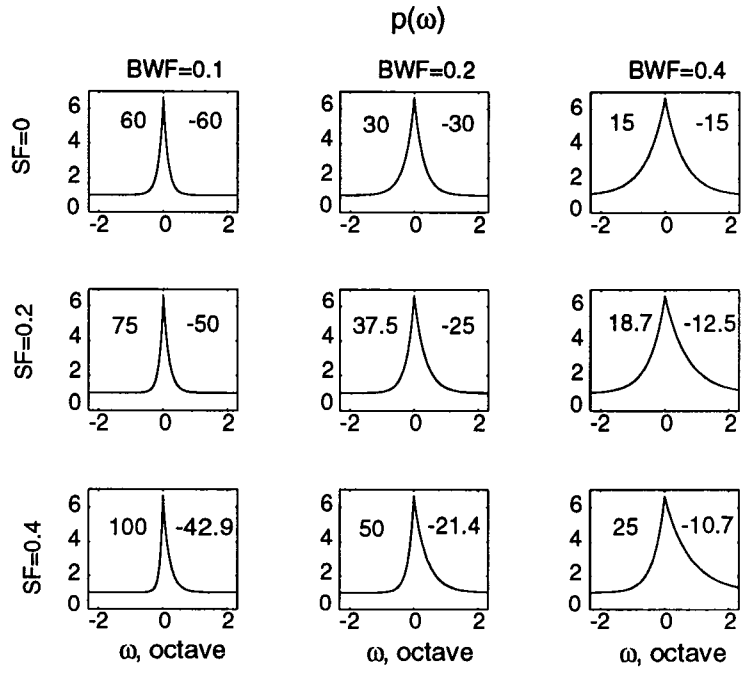

Figure 1: (b) Various peak profiles plotted on a linear amplitude axis. Columns share the same BWF's and rows share the same SF's. Corresponding left and right slope values (in dB/octave) are shown for each case.

BWF and SF values were also constrained by the need to ensure that the profile substantially decayed before reaching the edges of the base (at 0.2 and 5 kHz). Finally, the range of BWF and SF values tested corresponds to those that might be computed from the spectral envelope of speech sounds, as shown in Fig. 1(c).

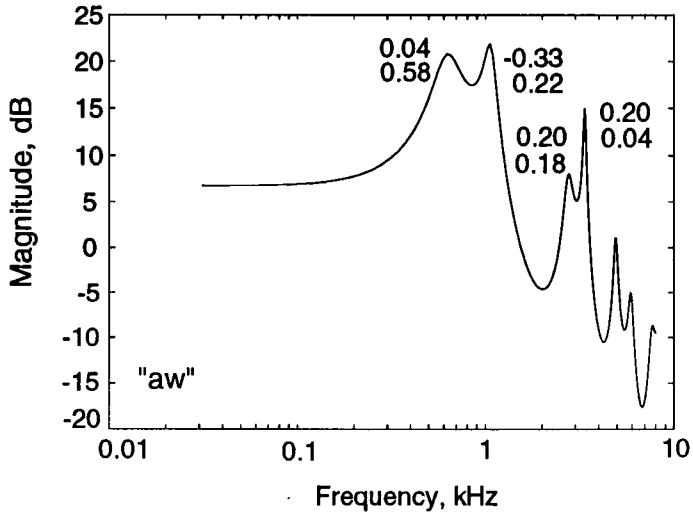

Figure 1: (c) SF's (top) and BWF's (in octaves, bottom) for the spectral peaks of a naturally spoken vowel "aw".

C. Ripple transform of the peak profile

According to the ripple analysis model [*Vranić-Sowers and Shamma*, 19xx], the detection of peak shape changes is based on the ripple transform representation of the peak. In order to predict perceptual thresholds for the **fdl-, pdl-**, and pedestal-type experiments, we need to examine the peak's ripple transform, $r(.)$, and specifically how BWF and SF are interpreted in this domain.

First, the ripple spectrum $P(\Omega)$ of the peak profile is for $\Omega > 0$ cycle/octave computed as:

$$P(\Omega) = |P(\Omega)|e^{j\theta} = \frac{a_{max}}{b}\frac{20\ \mathrm{BWF}}{3\ln 10\ M}\cdot$$

$$\frac{1}{1 + j\ 2\pi\Omega\ 20/(3\ \ln 10)\ \mathrm{SF}\ \mathrm{BWF} + (\pi\Omega\ 20/(3\ln 10)\ \mathrm{BWF})^2(1-\mathrm{SF}^2)},$$

where the magnitude of the ripple spectrum is:

$$|P(\Omega)| = \frac{a_{max}}{b}\frac{\mathrm{c}\ \mathrm{BWF}}{\pi\ M}\frac{1}{\sqrt{(1+\Omega^2\ (\mathrm{c}\ \mathrm{BWF})^2(1-\mathrm{SF}^2))^2 + \Omega^2(2\mathrm{c}\ \mathrm{SF}\ \mathrm{BWF})^2}},$$

c = 20 $\pi/(3\ \ln 10) \approx 9.1$ and $|P(0)| = 1 + \frac{a_{max}}{b} \frac{\text{c BWF}}{\pi\ M}$ (Fig. 2(a))[1]. Using this expression, the magnitude of the ripple transform, $r(\Omega_o)$, is computed from Eq. (4) in [*Vranić-Sowers and Shamma*, 19xx] and displayed in Fig. 2(b) for two symmetric peaks with different BWF's (0.1 and 0.4 octaves). Note that the steepest lowpass edges of the ripple transforms (marked by the dashed lines) are located roughly at $\Omega_o = 0.85$ and 3.3 cycle/octave.

II. THRESHOLD PREDICTIONS OF THE RIPPLE ANALYSIS MODEL

A. Predictions for fdl-type measurements (Dilation thresholds)

For a peak $p(\omega)$, a relative change in BWF ($\frac{\delta \text{BWF}}{\text{BWF}}$) is equivalent to dilating the peak by a factor $\alpha = \frac{1}{1+\frac{\delta \text{BWF}}{\text{BWF}}}$ to $p(\alpha\ \omega)$. In the ripple transform domain this corresponds to translating the magnitudes of the ripple spectrum and ripple transform of a peak (Sec. I B in [*Vranić-Sowers and Shamma*, 19xx]) by $\log_2 \alpha$ octave on the logarithmic Ω_o axis (Figs. 2).

Since the locations of the steepest lowpass edges of the ripple transforms of all peaks used here fall in the range Ω_o =0.85–7 cycle/octave, then the ripple analysis model (Δ curve in Fig. 3(c) in [*Vranić-Sowers and Shamma*, 19xx]) predicts that subjects should detect a 0.26 octave shift in $r(\Omega_o)$. Since we always increased BWF in our experiments (i.e., δBWF> 0 octave), then $\Delta = -0.26$ octave ($= \log_2 \alpha$), i.e., $\alpha = 0.83$. This corresponds to $\frac{\delta \text{BWF}}{\text{BWF}} = 0.2$, or a 20% increase in BWF *regardless* of the standard peak's bandwidth. This estimate is also independent of the peak's symmetry (SF) since the latter mostly reflects the phase (not the magnitude) of the ripple transform (see discussion below).

---

[1]Note that these expressions can be simplified for the range of parameters used in our experiments. For instance, for small SF's ($SF^2 \ll 0.5$) the magnitude is independent of the SF:

$$|P(\Omega)| \approx \frac{a_{max}}{b} \frac{\text{c BWF}}{\pi\ M} \frac{1}{1+\Omega^2\ (\text{c BWF})^2}.$$

For $SF^2 \ll 1$, the phase function is given by:

$$\tan(\theta(\Omega)) \approx \theta(\Omega) \approx \frac{\Omega\ (2\text{c BWF})}{1+\Omega^2\ (\text{c BWF})^2} \cdot \text{SF}$$

which becomes

$$\theta(\Omega) \approx \text{SF}$$

for $\Omega \approx \frac{1}{\text{c BWF}}$, i.e., around $\Omega = 0.3, 0.5, 1.1$ cycle/octave for BWF= 0.4, 0.2, 0.1 octaves, respectively. Note that these are the Ω's at which the magnitude of the ripple transform of the peak $r(\Omega_o)$ is maximum (Fig. 2(b)) and hence where the bulk of the profile energy lies. The correspondence above between the $\theta(\Omega)$ and SF is more analytically established in Appendix A.

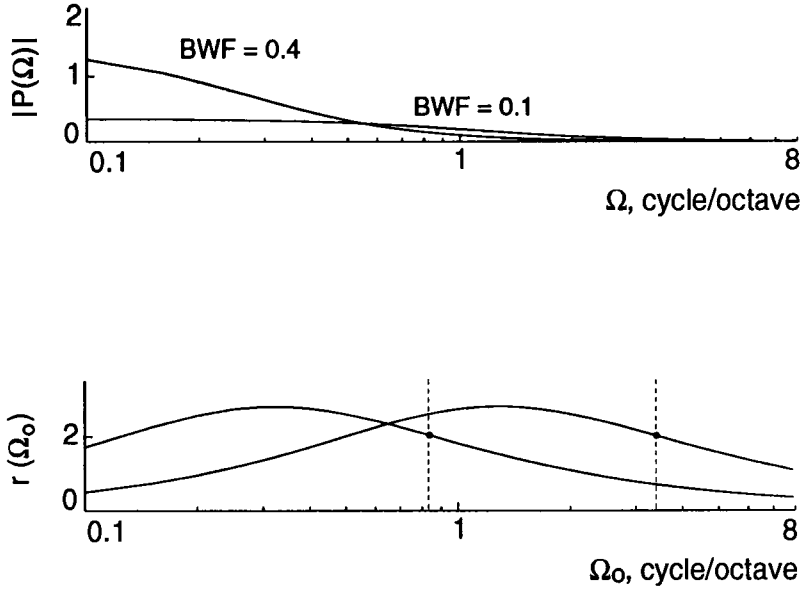

Figure 2: (a) Ripple spectra of peak profiles with $A_{max} = 15$ dB, SF's=0, and BWF's = 0.1 and 0.4 octaves. (b) Ripple transform magnitudes, $r(\Omega_o)$, of ripple spectra in (a). The effect of a BWF change is a shift (and not a change in shape) of the ripple transform along the logarithmic Ω_o axis. For example, a four-fold increase in BWF (from 0.1 to 0.4 octaves), i.e., $\frac{\delta \text{BWF}}{\text{BWF}} = 3$ or $\alpha = 0.25$ results in a ($\Delta = \log_2 \alpha =$) 2 octave downward shift in $r(\Omega_o)$.

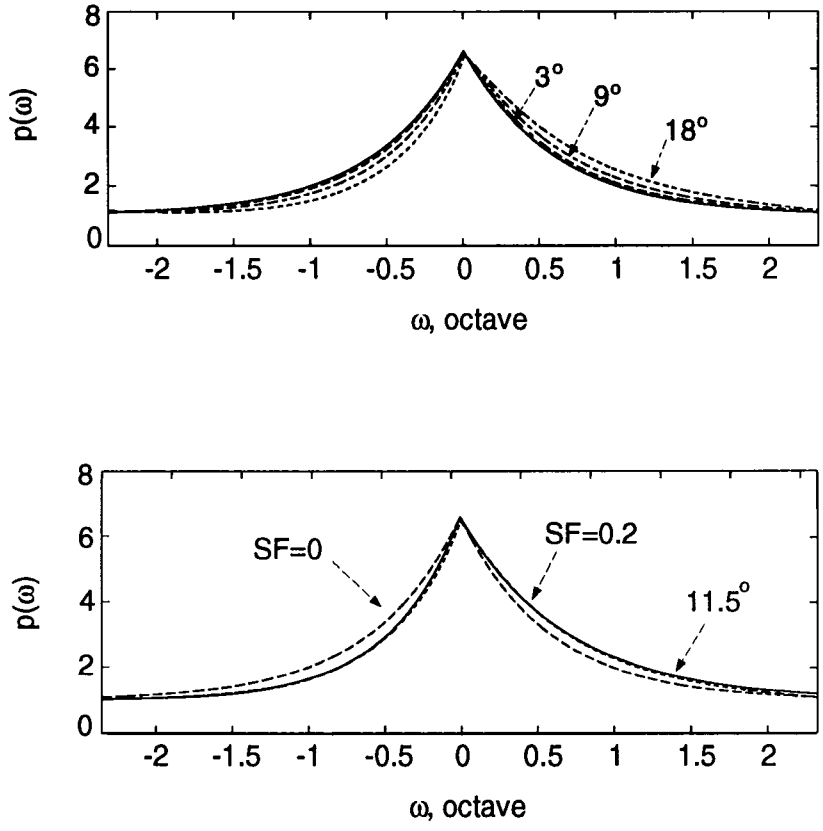

Figure 3: (a) The effect on a change in the symmetry of a peak profile (BWF = 0.4 octave, SF = 0) due to adding constant phases (3°, 9°, 18°, or 0.05, 0.16, 0.31 radians) to its Fourier transform. (b) Changes in the symmetry of a peak (BWF=0.4 octave, SF=0, dashed line) due to adding a constant phase $11.5^o = 0.2$ radians (dotted line) and due to changing the SF by δSF = 0.2 (solid line).

B. Predictions for pdl-type measurements (Ripple phase sensitivity)

Adding a small constant phase angle to all components of the peak ripple transform $r(\cdot)$ translates the phase function of the ripple transform and changes the peak's symmetry or SF, as demonstrated in Figs. 3. In Appendix A it is shown that δSF is approximately equal to the ripple phase of the peak profile (in radians). Hence, in all measurements reported here, the peak's ripple phase was manipulated simply by changing the SF directly (i.e., the slopes L and R around the peak) rather than via forward-inverse ripple transform operations.

The ripple phase sensitivity for peak profiles can be predicted from the ripple analysis model as follows. For the broader peaks (BWF $>$ 0.1 octave) the bulk of the ripple transform (Fig. 2(b)) lies in the low ripple range ($<$ 1 cycle/octave). Therefore, phase sensitivity is predicted to be constant at approximately 6^o or 0.1 radians (Fig. 4(b) in Part I, the 25 dB curve). Equivalently, subjects should be able to detect a SF change (δSF) of approximately 0.1. This threshold estimate would increase for the narrowest peak (BWF = 0.1 octave) as the ripple transform shifts upwards towards the range of $\Omega_o > 1$ cycle/octave. Note that, as for the **fdl-** type tests, none of these predictions depend on the standard's peak symmetry.

C. Predictions for pedestal-type measurements (Peak amplitude sensitivity)

The ripple analysis model is basically linear and hence pedestal–type experiments should yield comparable thresholds regardless of the exact shape of the spectral profile. The only data previously available for such experiments used a single component pedestal profile (Fig. 5.4 in [*Green*, 1988]). Specifically, thresholds ranged between –8 and –16 dB's for pedestals up to 24 dB larger than the base. The variability is attributed to masking effects depending on the spectral density in the vicinity of the signal [*Green*, 1988].

III. MEASURED THRESHOLDS FOR PEAK SHAPE CHANGES

A. Methods

The experiments are similar in methodology to previously reported profile analysis experiments ([*Bernstein and Green*, 1987; *Bernstein, Richards and Green*, 1987; *Green, Mason and Kidd*, 1984; *Kidd, Mason and Green*, 1986]). The specifics of the experimental procedures used are identical to those described in Part I (Sec. II B.2(i)) of this paper [*Vranić-Sowers and Shamma*, 19xx]. Again, the waveform was turned on 10 ms following the onset in order to suppress the large amplitudes due to zero phases.

The step size was defined in terms of a change in the right slope of the peak and it differed across the testing conditions, ranging from 0.3 dB/octave – 5.5 dB/octave.

Threshold measure was defined as the amount of change in BWF or SF needed for detection (for, respectively, a constant SF or BWF testing condition), i.e., δBWF or

δSF. In the case of BWF change tests, the normalized by the peak's BWF thresholds were used (i.e., δBWF/BWF).

The results reported are based on data from two to five normal hearing subjects, depending on the particular test.

B. Detection of change in bandwidth (Dilation thresholds)

Experiments here measured detectability of a dilation (stretching) of the spectral peak or, equivalently, of an increase in its BWF, while holding the peak symmetry constant. To recognize the signal, subjects reported listening to several different sound qualities, e.g., pitch and sharpness of sound. Some reported changing strategies depending on the testing conditions.

In the parameter range tested, dilation thresholds remained relatively constant at $\alpha \approx 0.8$ (or δBWF/BWF ≈ 0.22) regardless of standard's peak shape (Figs. 4). This result is consistent with predictions of the ripple analysis model discussed above in Sec. II A.

Thresholds only slightly decreased for higher peak amplitudes (i.e., > 15 dB in level), but increased sharply for lower amplitudes perhaps due to masking effects of the base upon the smaller peak profiles (Appendix B.1, Fig. B1). Thresholds were also relatively independent of spectral component density (Fig. B2).

Two conclusions can be drawn from the above results. First, the constancy of the dilation thresholds in the peak profiles is directly related to the constancy of the **fdl**'s in the $0.85 - 7$ cycle/octave range (Δ curve in Fig. 3(c) in [*Vranić-Sowers and Shamma*, 19xx]). Second, the measured dilation thresholds hold *regardless* of the exact details of the peak shape since the thresholds depend only on the shift and not on the shape of the ripple transform magnitude (Sec. II B.1 in [*Vranić-Sowers and Shamma*, 19xx]).

C. Detection of change in symmetry (Ripple phase sensitivity)

These experiments measured subjects' sensitivity to a change in peak symmetry while holding its BWF constant or, equivalently, a shift in the phase of the ripple transform of the peak profile. Subjects trained relatively quickly to distinguish signal from standard, reportedly based on pitch–like cues. This "pitch" effect is further explored in Sec. IV C.

In the parameter range tested, ripple phase sensitivity remained relatively constant at approximately 6^o (or $\delta SF \approx 0.11$) regardless of the peak shape (Figs. 5). There was, however, a consistent small increase in threshold as a function of decreasing BWF (Fig. 5(b)), especially at the narrowest peaks (BWF= 0.1 octave) where thresholds rose to 10^o (δSF ≈ 0.17).

Thresholds changed only slightly for different peak amplitudes and spectral component densities (Figs. B3 and B4, Appendix B.2). The major exception was the narrowest peak where decreasing spectral density caused detection thresholds to rise significantly.

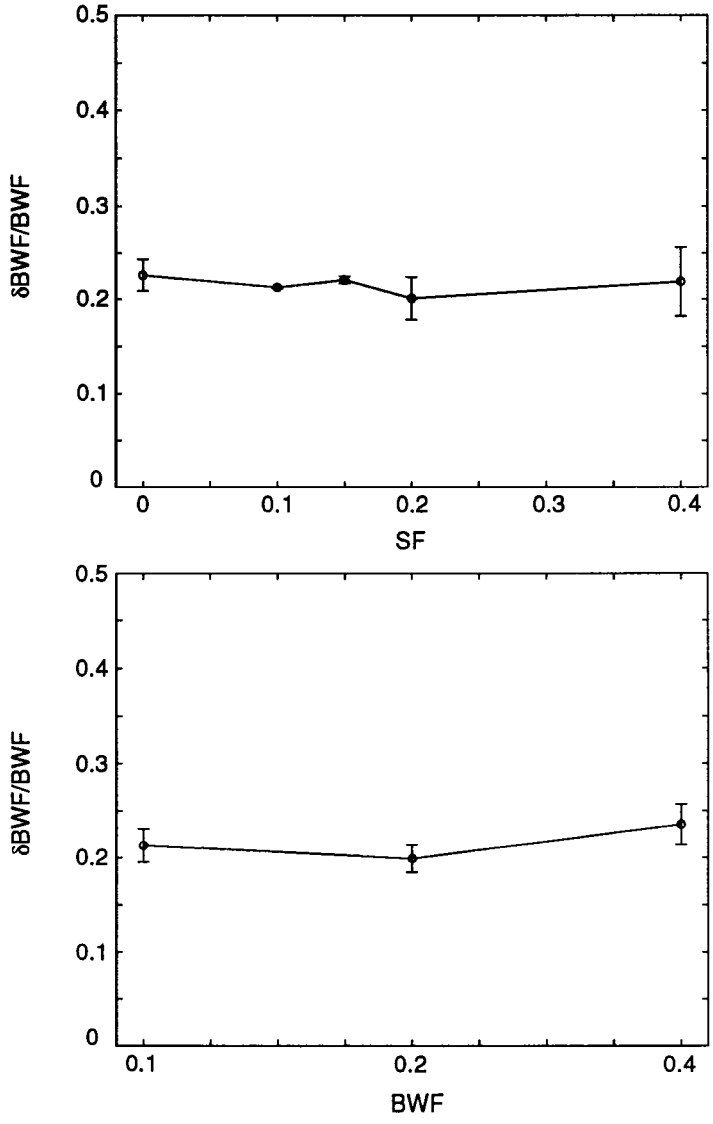

Figure 4: Bandwidth factor change detection thresholds, δBWF/BWF, for 41 frequency components and 15 dB peak level (which allowed the peak to be heard clearly), are averaged over three listeners and three BWF's (0.1, 0.2, 0.4 octaves) in (a) and five SF's (0, 0.1, 0.15, 0.2, 0.4) in (b). The error bars are the standard deviations of the means.

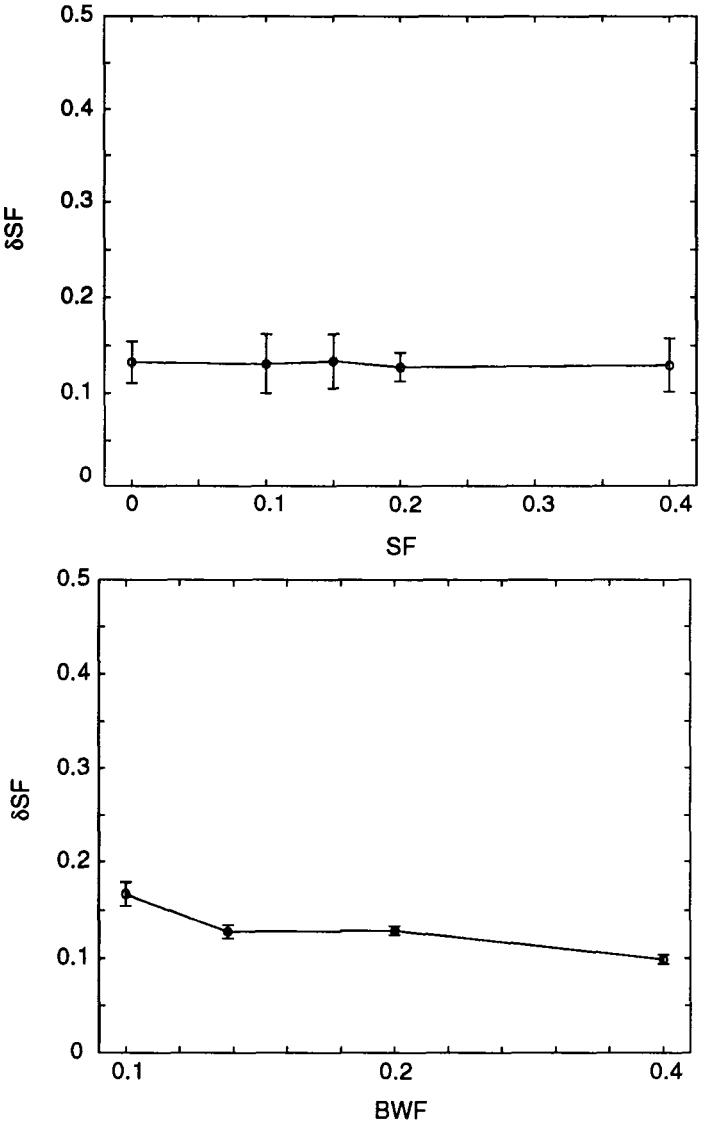

Figure 5: Symmetry factor change detection thresholds, δSF, for 41 component complex and 15 dB peak amplitude, are averaged over five subjects and four BWF's (0.1, 0.13, 0.2, 0.4 octaves) in (a) and five SF's (0, 0.1, 0.15, 0.2, 0.4) in (b). Note the δSF increase for the narrowest BWF in (b). The error bars are the standard deviations of the means.

Ripple phase sensitivity measurements shown here are similar to those previously obtained with ripple profiles (Sec. II B.2(iii) in Part I [*Vranić-Sowers and Shamma*, 19xx]), in that both exhibit a constant minimum threshold of approximately 6° at low ripple frequencies (or, equivalently, for broad peaks) which gradually rises at higher ripples (or narrow peaks). These results, therefore, are consistent with the predictions of the ripple analysis model.

D. Detection of change in peak amplitude (Peak amplitude sensitivity)

Thresholds for a change in the amplitude of the peak (test A in Fig. 6) were measured in the range –7 to –10 dB's (values are given in the parentheses in Fig. 6) for all peak standards. While they were independent of the SF's, thresholds were slightly lower for the narrowest peaks (BWF = 0.1 octave). These thresholds are comparable to those obtained with single component pedestals. They are also consistent with the notion that this linear ripple analysis model (which does not take into account explicitly the masking effects) may be an adequate first-order approximation for pedestal-type experiments with larger-than-base pedestal profiles.

This experiment also serves in a different way as a control to rebut the argument that dilation thresholds may simply reflect the detection of a change of total peak profile energy, rather than of bandwidth *per se*. This is because in all dilation tests (Sec. III B) the energy was not equalized as the peak bandwidth was altered. In this experiment, BWF was kept constant as the peak amplitude increased. So, if the two tasks were based on energy change, then the rms-thresholds should be comparable. The plots in Fig. 6 demonstrate that this is not the case, since rms-thresholds for dilation tests are uniformly lower by approximately 6 dB's, i.e., subjects are specifically sensitive to a change in peak bandwidth.

IV. THRESHOLD PREDICTIONS BY OTHER PROFILE ANALYSIS MODELS

In this section detection thresholds measured for peak and ripple profiles are compared to predictions from three different models of profile analysis: the independent channels model [*Durlach, Braida and Ito*, 1986], the maximum difference model [*Bernstein and Green*, 1987], and the Ewaif model [*Feth, O'Malley and Ramsey*, 1982; *Stover and Feth*, 1983]. The first two models operate on the profile directly and assume that profile changes are conveyed by independent channels distributed across the spectrum. The third model bases detection on a derived "pitch-like" measure (the Ewaif pitch) from the profile. The validity of predicted thresholds is judged based on the constancy of the $d'\sigma$ index (σ is the variance of the channels, see below) and the Ewaif pitch computed at perceptual thresholds.

A. The channel model

This model is described in detail in [*Durlach, Braida and Ito*, 1986; *Green*, 1988]. It combines information from N independent noisy channels whose variances (σ)

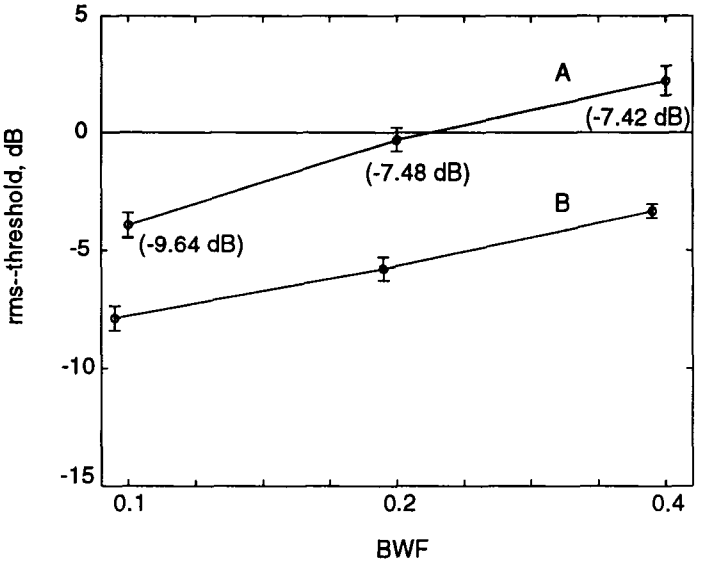

Figure 6: Detection thresholds for a peak level change (test A) compared to a BWF change (test B). The rms–threshold for the two tests is defined as 20 $\log \sqrt{\sum_{i=1}^{N}(\Delta p_i/p_i)^2}$, where Δp_i is the change in the amplitude of the i^{th} component at threshold, p_i is the amplitude of the i^{th} component in the standard, and N is the number of components. The values in the parentheses are computed as 20 $\log \Delta p_{N+1/2}/p_{N+1/2}$, where $p_{N+1/2}$ is the central component of the pedestal standard. Three subjects participated in this series and were tested at two SF's (0, 0.4) and three BWF's (0.1, 0.2, 0.4 octaves), for a 41 component complex and at 15 dB standard peak level.

are assumed to be constant. Some interdependence between the channel outputs is introduced because of the level randomization in the experiments. The uniform roving level distribution over a 20 dB range ($\sigma_R = 5.6$) is approximated by a normal distribution of $\sigma_R = 5$. Furthermore, it is assumed that the channel variances are such that $\sigma_R \cdot N \gg \sigma$. The level difference between the standard's and signal's i^{th} component is defined as $\Lambda_i = 20\ \log((p_i)_{signal}/(p_i)_{standard})$. These assumptions lead to $d' = \sqrt{(\sum \Lambda_i^2 - \frac{1}{N}(\sum \Lambda_i)^2)}/\sigma$. The numerator (or $d'\sigma$) was computed at perceptual thresholds for different testing conditions (Tables I) and at the limits of the error bars, in order to determine its sensitivity to threshold changes. Since no explicit σ values are used, absolute threshold values will not be predicted. Instead, we shall be mostly concerned with the trends in the data and with the relative threshold values for different profiles.

For δBWF tests all $d'\sigma$'s (with one exception) are comparable when considering the significant overlap due to the error bars (Table I(a)). Thus, the model predicts that dilation thresholds for peak profiles are constant regardless of the shape of the standard peak. This is consistent with the measured thresholds.

For δSF tests the stimuli are "balanced" (see [*Durlach, Braida and Ito*, 1986]) in that $\sum \Lambda_i \approx 0$ or at least $(\sum \Lambda_i)^2 \ll N \sum \Lambda_i^2$. Here, the channel model makes two erroneous predictions (Table I(b)): (1) As a function of SF it predicts a small consistent decrease in thresholds that is not evident in the data; (2) As a function of BWF it predicts that phase sensitivity improves with increasing BWF's, rather than being constant for broad peaks (BWF=0.2 and 0.4 octaves) as the data indicate.

Interestingly, the model is able to predict a constant phase sensitivity (Table I(c)) for low frequency ripples (< 1 cycle/octave) when applied to single ripple profiles discussed in Sec. II B.2 in [*Vranić-Sowers and Shamma*, 19xx]. It is unclear why this constancy of thresholds is not seen with the peak profile predictions[2].

B. The maximum difference model

The maximum difference model described in [*Bernstein and Green*, 1987] is based on detecting the largest difference between any pair of components in the signal, i.e., it uses only two channels in computing the thresholds. The model was derived from experimental results with flat standards and was defined accordingly for such tests. It predicts well the thresholds in a number of profile analysis tasks [*Bernstein and Green*, 1987]. In order to apply the model to the peak stimuli the computational scheme was slightly modified. For instance, we define the level difference between the i^{th} and j^{th} frequency component as $\Lambda_{i,j} = 20\ \log((p_i)_{signal}/(p_i)_{standard}) - 20\ \log((p_j)_{signal}/(p_j)_{standard})$. Also, contrary to the assumption of the original model ([*Bernstein and Green*, 1987]), we take the σ's to

[2]The $d\ \sigma'$ values were also computed using only 41 components, or in effect 41 independent channels. They were about half of the values reported in Table I(c) for 161 components and are, therefore, comparable to those for peak profiles.

$d'\sigma$ for δBWF test

SF	BWF (octave) 0.1	0.2	0.4	average
0	3.11 ±0.24	3.02 ±0.19	2.58 ±0.21	2.90
0.4	3.12 ±0.25	3.16 ±0.20	3.27 ±0.25	3.18
average	3.11	3.09	2.92	
δBWF/BWF threshold	21.5 ±1.8%	20.0 ±1.4%	23.6 ±2.1%	

$d'\sigma$ for δSF test

SF	BWF (octave) 0.1	0.2	0.4	average
0	2.96 ±0.19	2.88 ±0.13	3.97 ±0.18	3.27
0.4	3.36 ±0.22	3.22 ±0.15	4.33 ±0.20	3.64
average	3.16	3.05	4.15	
δSF threshold	0.16 ±0.01	0.11 ±0.005	0.11 ±0.005	

$d'\sigma$ for phase–ripple experiment

	ripple frequency (cycle/octave) 0.25	0.5	1	2	4	8
$d'\sigma$	9.59	10.44	8.89	9.47	19.0	19.58
pdl. 15 dB	8.09°	9.08°	7.53°	8.1°	16.22°	13.47°
$d'\sigma$	10.67	10.20	10.08	14.32	28.39	
pdl. 25 dB	5.39°	5.31°	5.11°	7.34°	11.53°	

Table I: $d'\sigma$ (dB) values for the "independent channels model" (Sec. IV A). (a) $d'\sigma$ for δBWF tests are evaluated at threshold and error bar limit values which are given at the bottom of each table. (For example, for BWF = 0.1 octave and SF= 0, δBWF/BWF = 21.5% with error bar limits of $\pm$ 1.8%, and the corresponding $d'\sigma = 3.11 \pm 0.24$.) Thresholds are taken from Fig. 4(b) (41 components and 15 dB peak level). (b) $d'\sigma$ values for δSF tests. The table is organized as Table I(a) with threshold values from Fig. 5(b) (41 components and 15 dB peak level). (c) $d'\sigma$ for **pdl** tests with ripple profiles for 15 dB and 25 dB ripple levels and thresholds from Fig. 4(b) in Part I (161 components). (The $d'\sigma$ values for 41 components, for ripple frequencies between 0.25 – 4 cycle/octave, are half of the values reported here for 161 components.)

be constant for all channels and, hence, the largest d' is defined by the largest $\Lambda_{i,j}$ (defined as Λ).

For δBWF tests Λ is approximately constant for all SF's and BWF's (Table II(a)). Therefore, the model predicts well the perceptual trends assuming constant σ's across all spectral regions. If σ's are allowed to increase towards the edges (as in [*Bernstein and Green*, 1987]), d' would decrease with increasing BWF predicting erroneously higher thresholds for these conditions.

For δSF tests the model makes two erroneous predictions (Table II(b)): (1) Like the channel model it predicts a small consistent decrease in thresholds as a function of SF that is not evident in the data; (2) It predicts a constant phase sensitivity as a function of BWF for all peaks, i.e., it does not account for the increase in δSF thresholds for the narrowest peaks (BWF = 0.1 octave).

The model is also able to predict a constant phase sensitivity for low frequency ripples (< 1 cycle/octave) when applied to the single ripple (Table II(c)). Therefore, unlike the channel model above, this model consistently predicts the constant phase property for both the ripple and peak profiles. The failure of the model to predict the declining phase sensitivity at high ripple frequencies is likely because it does not explicitly incorporate data such as the ripple-**pdl** in Fig. 4(b) in [*Vranić-Sowers and Shamma*, 19xx].

C. The Ewaif model

Numerous experimental results have suggested that the detection of spectral shape changes may in some cases be effectively mediated by pitch cues associated with these spectral changes ([*Berg, Nguyen and Green*, 1992; *Feth, O'Malley and Ramsey*, 1982; *Richards, Onsan and Green*, 1989; *Stover and Feth*, 1983]). In order to assess the possible contribution of such a pitch cue in our tests, we measured the effect on thresholds of randomizing peak locations – a procedure which in effect destroys the pitch cue. The change in thresholds was then compared to what would be predicted from the theoretical strength of the pitch cue computed for each test using the so-called Ewaif model [*Stover and Feth*, 1983].

1. Stimulus

The entire spectral content was randomly shifted in order to prevent listeners from using standard's and signal's complex pitches for spectral shape change detection. Frequency shift was achieved by randomly changing the sampling time in a range of 40 μs to 45 μs in steps of 0.5 μs. This amounts to shifting the central component from 1000 Hz to 889 Hz and all the other components accordingly to preserve the frequency spacing.

The measured thresholds and the corresponding Ewaif pitches are presented in Tables III. The Ewaif pitches were computed for zero phases which corresponds to our stimulus condition.

Λ for δBWF test

SF	BWF (octave) 0.1	0.2	0.4	average
0	1.43	1.37	1.59	1.46
0.4	1.45	1.37	1.59	1.47
average	1.44	1.37	1.59	
δBWF/BWF threshold	21.5%	20%	23.6%	

Λ for δSF test

SF	BWF (octave) 0.1	0.2	0.4	average
0	2.39	1.65	1.66	1.90
0.4	3.07	2.01	2.09	2.10
average	2.73	1.81	1.87	
δSF threshold	0.16	0.11	0.11	

Λ for phase–ripple experiment

	ripple frequency (cycle/octave) 0.25	0.5	1	2	4	8
Λ	2.12	2.38	1.97	2.12	4.23	11.11
pdl, 15 dB	8.09°	9.08°	7.53°	8.1°	16.22°	43.17°
Λ	2.35	2.32	2.23	3.16	6.32	
pdl, 25 dB	5.39°	5.31°	5.11°	7.34°	14.53°	

Table II: Maximal difference levels, Λ (dB), for the "maximal difference model" (Sec. IV B). Tables are organized as Tables I.

2. Assessing the data using the Ewaif model

In order to assess the amount of a pitch cue contribution to the detection of changes in our stimulus, the following two arguments (from [*Richards, Onsan and Green*, 1989]) are used: 1) If the detection process relies primarily on a pitch cue (as defined by the Ewaif model), then some minimal pitch difference, ΔF ([*Feth and Stover*, 1987]), or relative pitch difference, $\Delta F/F_{sta}$ ([*Richards, Onsan and Green*, 1989]), is necessary for detection. Therefore, ΔF or $\Delta F/F_{sta}$ at perceptual thresholds should remain relatively constant.

2) If a threshold deterioration occurs due to the uncertainty in the randomized signal and not due to the pitch differences across the testing conditions, then it should be uniform across all conditions. Otherwise, the deterioration probably reflects the effective contribution of the pitch cue. This is evaluated by the change in values of the NR–R in Tables III.

3. Results and discussion

(i) Effects on detection of BWF changes (Table III(a))

The ΔF and $\Delta F/F_{sta}$ values vary greatly (approximately 7-fold) across the SF's and BWF's. Note also a change in sign of ΔF across various testing conditions. This strongly suggests that the pitch cue plays a minimal role in this discrimination task. Furthermore, a near uniform increase of the thresholds when the signal is randomized supports the notion that it is due to an uncertainty effect rather than an abolishment of a pitch cue.

(ii) Effects on detection of SF changes (Table III(b))

With respect to the first argument above, it is clear from the ΔF and $\Delta F/F_{sta}$ values in Table III(b) that not all pitch cues are equal at threshold, since both increase approximately 4-fold over the SF's and BWF's tested. However, the rise in δSF for the narrowest peak might be due to decreasing pitch cue. This is further supported by the data with respect to the second argument, namely that the randomization affects only the δSF thresholds of the narrower peaks. Therefore, the evidence here suggest that the pitch cue may be effective only for these peaks.

V. DISCUSSION

We measured subjects' ability to detect changes in the shape of peak profiles under various conditions. Specifically, our goal was to demonstrate that, for profiles that satisfy the two constraints outlined in Sec. IV B of [*Vranić-Sowers and Shamma*, 19xx], thresholds for dilating the profile, shifting its ripple phase, or changing its overall amplitude, are rather independent of the details of the profile. More generally, these manipulations can be interpreted and thresholds predicted within the unified framework of the ripple analysis model.

	BWF (octave)					
	0.1		0.2		0.4	
	SF					
δBWF test	0	0.4	0	0.4	0	0.4
NR	0.30	0.31	0.32	0.25	0.23	0.23
R	0.43	0.42	0.62	0.53	0.37	0.36
-(NR R)	0.13	0.11	0.30	0.28	0.14	0.13
F_{sta}	1290.52	1327.40	1227.73	1329.10	1223.27	1430.59
F_{sig}	1243.44	1318.03	1216.00	1377.66	1255.29	1505.61
$\Delta F=F_{sta}-F_{sig}$	38.65	9.66	11.69	-49.96	-26.78	-73.16
$\Delta F/F_{sta} \cdot 100$	2.99	0.73	0.95	-3 76	-2.19	-5.11

	BWF (octave)					
	0.1		0.2		0.4	
	SF					
δSF test	0	0 4	0	0.4	0	0.4
NR	0 27	0.27	0.13	0.15	0.13	0.11
R	0 36	0.44	0.27	0.23	0 17	0.12
-(NR R)	0.09	0.17	0.14	0.08	0.04	0.01
F_{sta}	1290 52	1327.40	1227.73	1329.10	1223 27	1430.59
F_{sig}	1315.58	1345.59	1258.54	1369.30	1293.42	1495.99
$\Delta F=F_{sta}-F_{sig}$	-25 04	-18.19	-30.83	-40.25	-70.13	-65.39
$\Delta F/F_{sta} \cdot 100$	-1.94	-1 37	-2 51	-3.03	-5.73	-4.57

Table III: (a) δBWF/BWF and (b) δSF detection thresholds for non-randomized (NR) and randomized (R) spectra (Sec. IV C). The tables are organized in the same way. The first two rows are the NR and R thresholds. The third row is the difference of the first two. The forth and fifth rows are the computed Ewaif pitches of standard (F_{sta}) and signal (F_{sig}) at perceptual threshold levels for NR condition and zero-phase components. The ΔF row is $\Delta F = F_{sta}-F_{sig}$. The last row is the relative pitch difference, $\Delta F/F_{sta}$ in percentage. Note in (a) a change in sign of ΔF across various testing conditions, which may explain the change in strategies that our subjects reported in performing δBWF task.
Three subjects participated in δBWF and two in δSF series. They were tested at two SF's (0, 0.4) and three BWF's (0.1, 0.2, 0.4 octaves) for 41 spectral density complexes and at 15 dB peak level.

The results obtained seem on the whole to confirm these hypotheses. Thus, dilation thresholds for peak and single ripple profiles (**fdl's**) are similar (Secs. III B and II A, respectively). Thresholds for changes in peak symmetry are also readily interpretable as ripple phase sensitivity and are close to those obtained from changing the phase of ripple profiles (Secs. III C and II B, respectively).

Also examined in this paper is the ability of other profile analysis models to account for the measured threshold values and trends. The channel model fails mostly in the phase sensitivity tests (δSF and **pdl** test for ripple profiles), where its prediction of trends are at variance with the measured results. The maximum difference model faired the best among the three alternatives considered. On the whole it predicts correctly the trends in all dilation thresholds and most phase sensitivity tests. The most obvious flaw is its inability to predict the deterioration of phase sensitivity for higher ripple frequencies and narrow peak profiles. It is conceivable that the model can be modified to take these measurements into account. For example, a suitable smoothing of the spectral profile may reduce the effective amplitude of the higher ripple components, in effect raising their thresholds. Finally, the Ewaif model cannot account for the δBWF thresholds and accounts only partially for the δSF measurements. Clearly, these criticisms apply only to the specific formulations of the models considered here and it is possible that future modifications will improve their predictions significantly.

Note, however, that the maximum difference model was originally developed specifically to predict **idl**-type tests and not the **fdl-** and **pdl**-type tests discussed here. Therefore, a better comparison of the ripple analysis and the maximum difference models might be to account for the detection threshold of a profile composed of several ripples that do not appreciably interact within the same filter (e.g., separated by more than an octave). For different phases of the ripples the shape of the profile changes and so too the predicted thresholds of the maximum difference model. In contrast, the ripple analysis model predicts that detection thresholds are independent of the relative phases of the ripples. A specific example of such a profile is the square wave which is composed of a large fundamental ripple and smaller odd harmonics. The maximum difference model predicts the threshold based on the amplitude of the square wave, whereas the ripple analysis model predicts it based on the amplitude of the fundamental (largest) ripple component. The two amplitudes differ by a small (hopefully measurable) factor of $4/\pi$.

In summary, the ripple analysis model is able to integrate efficiently data from a diverse set of profile analysis tests. It also provides a descriptive framework and a computationally tractable formulation to conceive of and test new hypotheses. But perhaps the most important impetus for pursuing this type of profile analysis model is the recent physiological findings on the functional organization of the auditory cortex [*Calhoun and Schreiner*, 1993; *Shamma, Versnel and Kowalski*, 1993]. These results support the notion that the auditory system performs a ripple analysis of

the spectral profile via ripple frequency and phase selective filters. The linear ripple analysis model presented here is a simplified formulation of this type of auditory processing.

ACKNOWLEDGMENTS

This work was supported by grants from the Air Force Office of Scientific Research, The Office of Naval Research, and the National Science Foundation (NSFD CDR8803012). The authors are members of the Institute for Systems Research. We are grateful to Dr. David Green and two anonymous reviewers for extensive reviews and helpful suggestions on the manuscripts, and to Daniel Naar from the Apple Corporation for valuable discussions.

Appendix A Adding a constant phase to the ripple spectrum of the profile

Consider the profile $p(\omega)$ whose Fourier transform is $P(\Omega)$:

$$p(\omega) = \frac{1}{2\pi}\int_{-\infty}^{\infty} P(\Omega)e^{j2\pi\Omega\omega}d(2\pi\Omega).$$

Adding a constant phase angle θ_o to all the transform components changes the profile to:

$$p_{\theta_o}(\omega) = \int_{-\infty}^{0} P(\Omega)e^{j\theta_o}e^{j2\pi\Omega\omega}d\Omega + \int_{0}^{\infty} P(\Omega)e^{-j\theta_o}e^{j2\pi\Omega\omega}d\Omega,$$

where the integral is split to emphasize that the phase function (added to negative frequencies and subtracted from positive frequencies) must be odd as a function of Ω in order for p_{θ_o} to remain real. This expression can be simplified further by substituting $e^{\pm j\theta_o} = \cos(\theta_o) \pm j\sin(\theta_o)$, and collecting terms:

$$p_{\theta_o}(\omega) = \cos(\theta_o)\int_{-\infty}^{\infty} P(\Omega)e^{j2\pi\Omega\omega}d\Omega - \sin(\theta_o)\int_{-\infty}^{\infty} jP(\Omega)\cdot sign(\Omega)\cdot e^{j2\pi\Omega\omega}d\Omega.$$

Therefore,

$$p_{\theta_o}(\omega) = \cos(\theta_o)p(\omega) + \sin(\theta_o)\mathcal{H}(p(\omega)),$$

where $\mathcal{H}(p(\omega))$ is the so-called Hilbert transform of $p(\omega)$. This is the expression used in computing the profiles in Fig. 3(a). A simpler expression can be used for the case of small θ_o ($\cos(\theta_o) \approx 1$ and $\sin(\theta_o) \approx \theta_o$):

$$p_{\theta_o}(\omega) = p(\omega) + \theta_o\mathcal{H}(p(\omega)). \tag{A1}$$

Another way of changing the symmetry of the peak $p(\omega)$ is by changing its SF by some δSF. The new tilted peak is:

$$p_{\delta\mathrm{SF}}(\omega) = b + a_{max}\ 10^{\frac{-6}{20\ \mathrm{BWF}}\frac{1}{1+\mathrm{SF}+\delta\mathrm{SF}}(\omega-\omega_o)} = b + a_{max}\ 10^{\frac{R}{20\ (1+\frac{\delta\mathrm{SF}}{1+\mathrm{SF}})}(\omega-\omega_o)}$$

$$\approx b + a_{max}\ 10^{\frac{R}{20}(1-\frac{\delta\mathrm{SF}}{1+\mathrm{SF}})(\omega-\omega_o)}$$

where $\omega \geq \omega_o$ and the approximation holds for $\delta\mathrm{SF} \ll 1 + \mathrm{SF}$. To simplify the algebra, let the peak be centered at $\omega_o = 0$ with $b = 1$, and let the starting peak be symmetric ($\mathrm{SF} = 0$) with slopes S (defined in Sec. I A). Then:

$$p_{\delta\mathrm{SF}}(\omega) = p(\omega) + a_{max}\ 10^{\frac{S}{20}\omega}\ (10^{\frac{|S|}{20}\ \delta\mathrm{SF}\ \omega} - 1)$$

$$= p(\omega) + (p(\omega) - 1)\ (e^{\frac{|S|}{20}\ \delta\mathrm{SF}\ \omega\ \ln 10} - 1)$$

$$\approx p(\omega) + \delta\mathrm{SF} \cdot [(p(\omega) - 1) \cdot (|S|\ \omega) \cdot \ln 10/20]. \qquad \text{(A2)}$$

Comparing the Eqs. (A1) and (A2), it is evident that to interpret δSF as equal to the ripple phase shift θ_o, we must have:

$$\mathcal{H}(p(\omega)) \approx (p(\omega) - 1) \cdot (|S|\ \omega) \cdot \ln 10/20. \qquad \text{(A3)}$$

This equivalence is demonstrated in Fig. A1 where the two expressions are plotted together. The correspondence between $p_{\delta\mathrm{SF}}(\omega)$ and $p_{\theta_o}(\omega)$ is further illustrated in Figs. 3 (text).

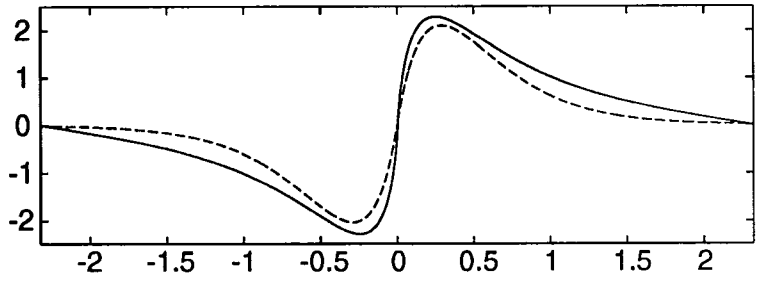

Figure A1: Comparing the two sides of Eq. (A3) for a peak with SF=0, BWF=0.2 octave, and A_{max} = 15 dB amplitude (or $b + a_{max}$ = 6.62). The solid line is the Hilbert transform and the dashed line is the right-hand side of the Eq. (A3).

Appendix B Dependence on peak amplitude and spectral density

1. Detection of change in bandwidth

(i) Dependence on peak amplitude

The dependence of δBWF/BWF thresholds on peak levels was examined using 10 dB, 15 dB , and 20 dB peak amplitudes. The average results of three subjects are shown as a function of SF and then as a function of BWF in Figs. B1(a) and (b), respectively. (One of the three subjects also participated in δBWF tests reported in Sec. III B.)

The plots confirm that, at a particular level, the δBWF/BWF threshold is largely independent of peak shape. However, thresholds do vary as a function of peak level but mostly at lower peak levels. For instance, on average, the rate of threshold rise in going from 20 dB to 15 dB peaks is less than half of that seen between 15 dB and 10 dB peaks.

(ii) Spectral density dependence

These experiments explored threshold dependence on the spectral density of the complex while keeping total base bandwidth constant (0.2–5 kHz). Peak level was kept at 15 dB level and 11, 21, and 41 component complexes were used. The average results of three subjects are presented in Figs. B2 as a function of SF in (a) and BWF in (b).

The δBWF/BWF thresholds remain constant for almost all conditions tested, i.e., regardless of peak shape and spectral density. The one obvious exception is at the broadest peak for the 11 component case, where thresholds increase significantly.

2. Detection of change in symmetry

(i) Dependence on peak amplitude

These experiments tested δSF threshold dependence on peak amplitude for various testing conditions (Figs. B3). The data are averaged over the BWF's in Fig. B3(a) and over the SF's in Fig. B3(b) for each of the peak levels.

Two conclusions can be derived from these data: (1) The same trends described earlier hold regardless of peak levels. Thus, except for the narrowest peak, all δSF thresholds are the same regardless of peak shapes studied. Note that on average, the three subjects tested here exhibited uniformly higher thresholds than the earlier five in Sec. III C. (One of the subjects participated in δSF tests reported in Sec. III C.) (2) δSF thresholds (as a function of BWF) deteriorate faster at the narrowest than other peaks with decreasing peak level (Fig. B3(b)). This rise is largely responsible for the upward shift in the mean of δSF's (as a function of SF, Fig. 3(a)) for smaller

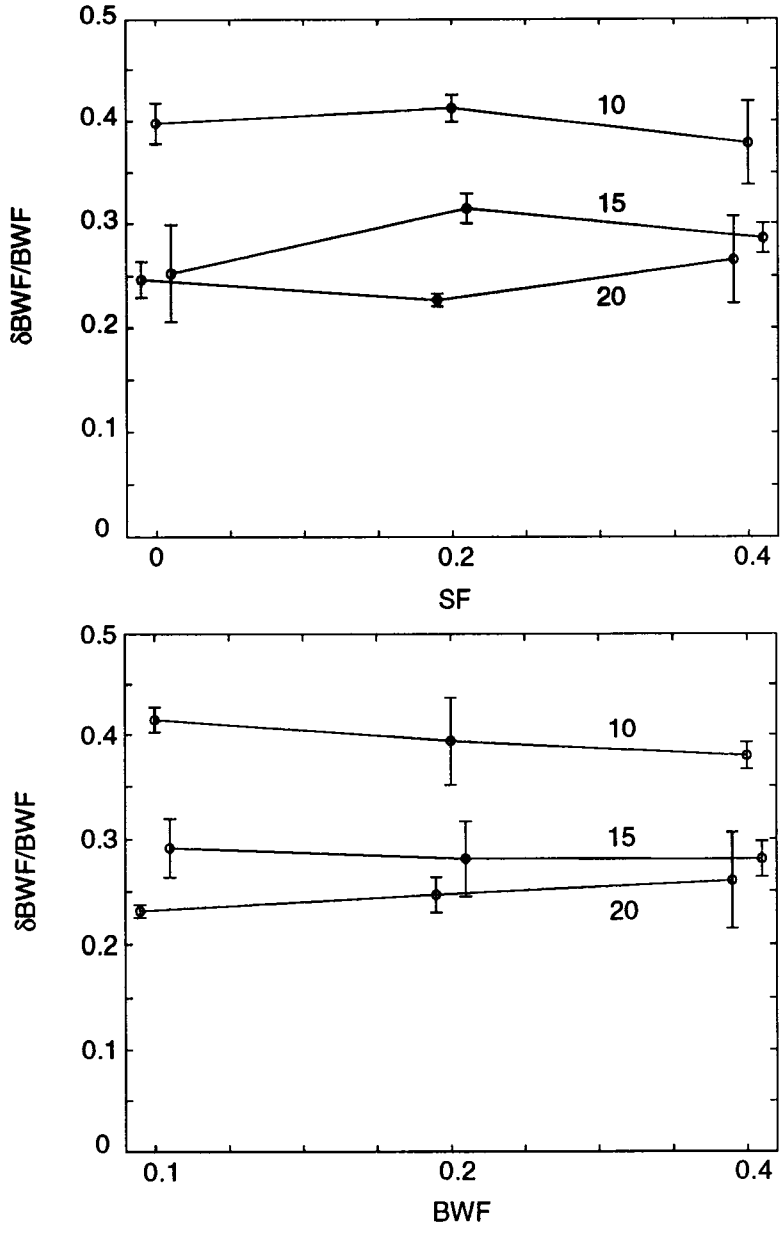

Figure B1: Bandwidth factor change detection thresholds, δBWF/BWF, for 41 component complex were measured for three subjects over the following conditions: three SF's (0, 0.2, 0.4), three BWF's (0.1, 0.2, 0.4 octaves), and at three peak levels (A_{max} = 10 dB, 15 dB, 20 dB). The δBWF/BWF thresholds are shown as a function of SF in (a) and BWF in (b). Points are offset along the abscissa for clarity.

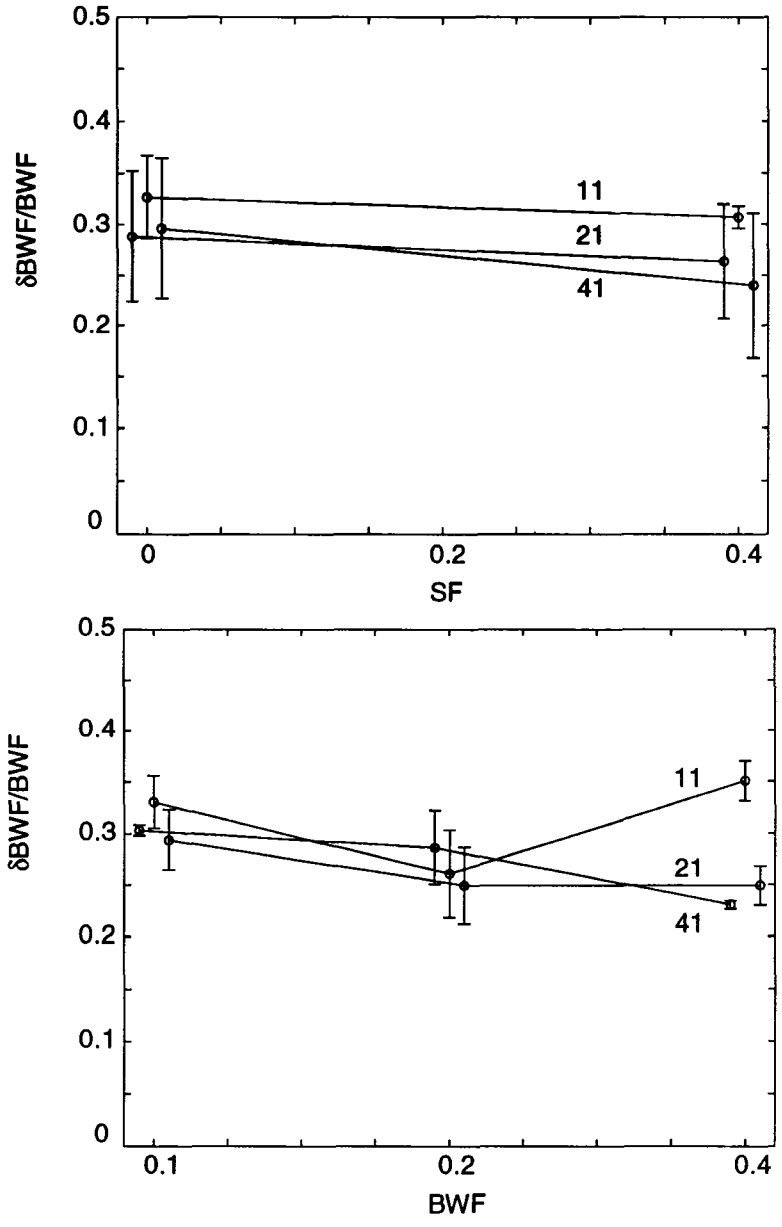

Figure B2: δBWF/BWF thresholds for 41, 21, and 11 component complexes and 15 dB peak level are averaged over three subjects and three BWF's (0.1, 0.2, 0.4 octaves) in (a) and two SF's (0, 0.4) in (b). Threshold is independent of spectral density for all but the broadest BWF, where it increases for the 11 component case.

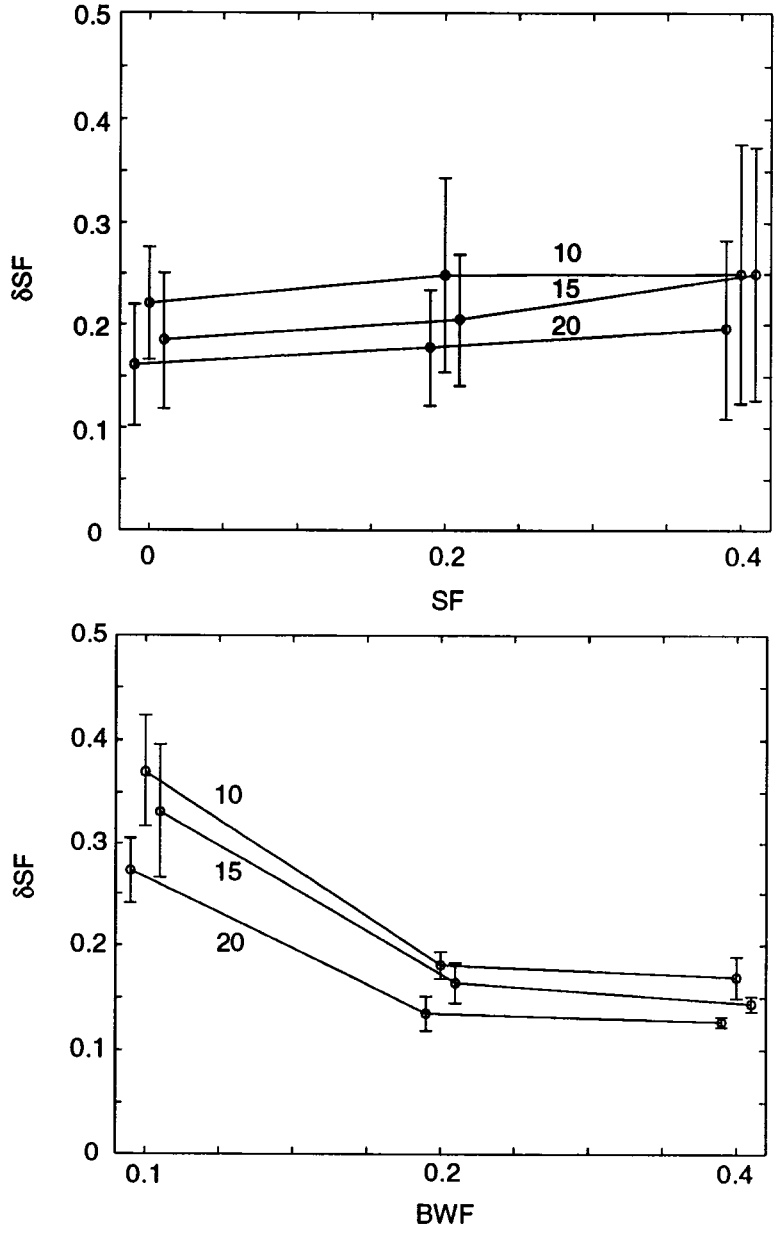

Figure B3: Symmetry factor change detection thresholds, δSF, for 41 component complex and three peak amplitudes (10 dB, 15 dB, 20 dB). At each peak level the data are averaged over three subjects and three BWF's (0.1, 0.2, 0.4 octaves) in (a) and three SF's (0, 0.2, 0.4) in (b). The large error bars in (a) are due to the δSF threshold increase for the narrowest peak (BWF=0.1 octave) seen in (b). Points are slightly offset along the abscissa for clarity.

peak levels. The overall slight rise in thresholds may reflect the masking of the peak by the base, which presumably increases for lower peak levels.

(ii) Spectral density dependence

Once again, all δSF values and trends described earlier largely hold regardless of spectral densities (Figs. B4). The most prominent change in δSF thresholds occurs as a function of spectral density at the narrowest peak (Fig. B4(b)). The threshold here deteriorates rapidly as the spectral density decreases and, as in Fig. B3(a), it is largely this accelerated rise that is responsible for the upward shifts in the mean of δSF in Fig. B4(a).

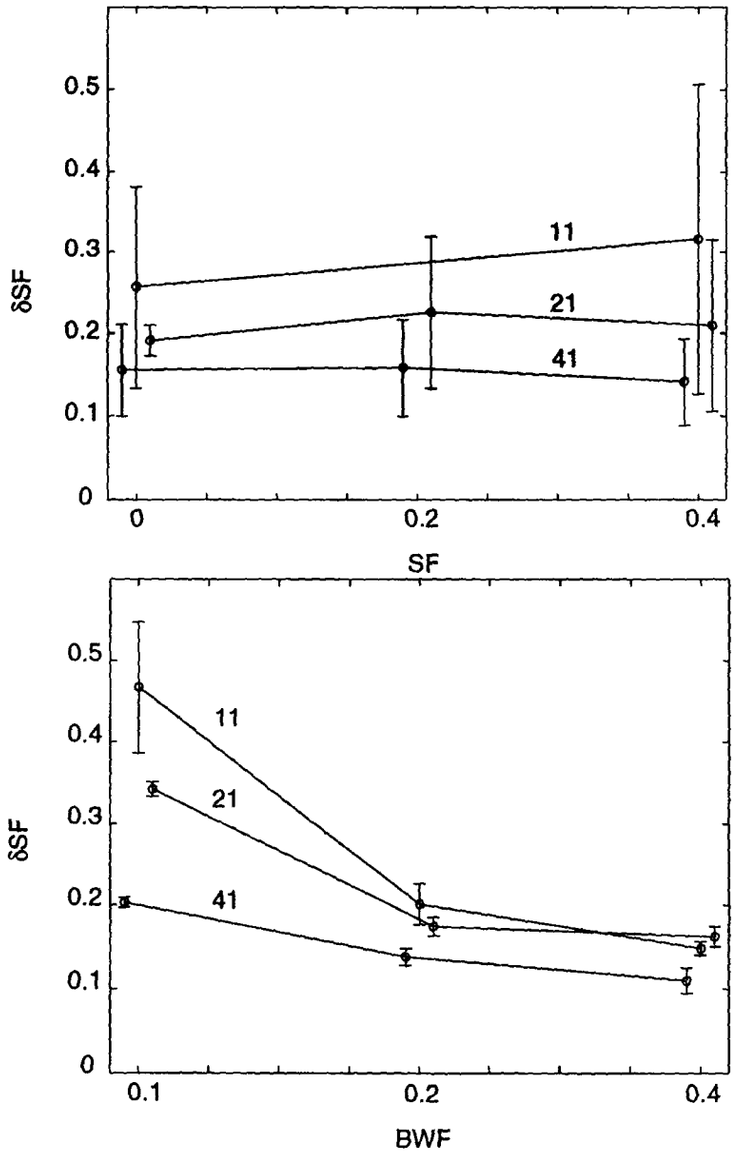

Figure B4: δSF thresholds for 41, 21, and 11 component complexes and 15 dB peak level are averaged over four subjects and three BWF's (0.1, 0.2, 0.4 octaves) in (a) and three SF's (0, 0.2, 0.4) for 41 and 21 component tests and two SF's (0, 0.4) for 11 component case in (b). As in Fig. B3, the large error bars in (a) are due to δSF increase for the narrowest peak seen in (b). Note that in (b), most δSF changes with spectral density occur at the narrowest peak.

REFERENCES

Berg, B. G., Q. T. Nguyen and D. M. Green, Discrimination of narrow-band spectra. I: Spectral weights and pitch cues, *J. Acoust. Soc. Am.*, *92*, 1911–1918, 1992.

Bernstein, L. R. and D. M. Green, Detection of simple and complex changes of spectral shape, *J. Acoust. Soc. Am.*, *82(5)*, 1587–1592, 1987.

Bernstein, L. R., V. M. Richards and D. M. Green, in *Auditory Processing of Complex Sounds: The detection of spectral shape change*, pp. 6–15, Lawrence Erlbaum Associates, Inc., New Jersey, 1987.

Calhoun, B. M. and C. E. Schreiner, Spatial frequency filters in cat auditory cortex, *Neurosc. Meeting, November*, *19*, 581.8, 1993.

Durlach, N. I., L. D. Braida and Y. Ito, Towards a model for discrimination of broadband signals, *J. Acoust. Soc. Am.*, *80 (1)*, 63–72, 1986.

Feth, L. L., H. O'Malley and J. J. Ramsey, Pitch of unresolved two-component complex tones, *J. Acoust. Soc. Am.*, *72*, 1403–1412, 1982.

Feth, L. L. and L. J. Stover, in *Auditory Processing of Complex Sounds: Demodulation processes in auditory perception*, pp. 76–86, Lawrence Erlbaum Associates, Inc., New Jersey, 1987.

Green, D. M., 'Frequency' and the detection of spectral shape change, in *Auditory Frequency Selectivity*, edited by B. C. J. Moore and R. D. Patterson, pp. 351–359, Plenum Press, Cambridge, 1986.

Green, D. M., in *Profile Analysis*, Oxford Press, New York, 1988.

Green, D. M. and C. R. Mason, Auditory Profile Analysis: Frequency, Phase, and Weber's Law, *J. Acoust. Soc. Am.*, *77*, 1155–1161, 1985.

Green, D. M., C. R. Mason and G. Kidd, Profile Analysis: Critical Bands and Duration, *J. Acoust. Soc. Am.*, *75*, 1163–1167, 1984.

Hillier, D. A., Auditory processing of sinusoidal spectral envelopes, Ph.D. Dissertation, The Washington University and Severn Institute, 1991.

Kidd, G. J., C. R. Mason and D. M. Green, Auditory profile analysis of irregular sound spectra, *J. Acoust. Soc. Am.*, *79*, 1045–1053, 1986.

Richards, V. M., Z. A. Onsan and D. M. Green, Auditory profile analysis: Potential pitch cues, 1989.

Shamma, S. A., H. Versnel and N. A. Kowalski, Organization of Primary Auditory Cortex evident in responses to rippled complex sound stimuli, *Neurosc. Meeting, November*, *19*, 581.9, 1993.

Stover, L. J. and L. L. Feth, Pitch of narrow-band signals, *J. Acoust. Soc. Am.*, *73*, 1701–1707, 1983.

Vranić-Sowers, S. and S. A. Shamma, Representation of spectral profiles in the auditory system. I: A ripple analysis model, *J. Acoust. Soc. Am. (submitted)*, 19xx .